Cement & Concrete Composites 33 (2011) 680–693

Contents lists available at ScienceDirect

Cement & Concrete Composites

journal homepage: www.elsevier.com/locate/cemconcomp

Relating ultrasonic measurements on fresh concrete with mineral additions to the microstructure development simulated by CEMHYD3D

Nicolas Robeyst [a], Christian U. Grosse [b], Nele De Belie [a,*]

[a] Magnel Laboratory for Concrete Research, Ghent University, Department of Structural Engineering, Technologiepark Zwijnaarde 904, B-9052 Ghent, Belgium
[b] Non-destructive Testing Lab, Center for Building Materials, Technische Universität München, Baumbachstr. 7, D-81245 Munich, Germany

ARTICLE INFO

Article history:
Received 29 January 2010
Received in revised form 3 January 2011
Accepted 11 March 2011
Available online 21 March 2011

Keywords:
Ultrasonic
Fresh concrete
Modelling
N-PLS
Mineral additions
Microstructure development

ABSTRACT

Ultrasonic measurements can be used to monitor concrete setting. To relate these measurements to fundamental changes in the cement paste, the results have been compared to the microstructure development as simulated with an adjusted version of the pixel model CEMHYD3D. The adjustments were validated by comparison with results of isothermal calorimetry, electron microscopy and thermal analysis. Mixtures in which the Portland cement was replaced by different dosages of blast-furnace slag and fly ash were tested. A multi-variate and multi-way regression was then performed between the ultrasonic results and the microstructure quantities.

For most microstructure parameters, the smallest difference between the simulated and predicted values is achieved with the models starting from the ultrasound frequency spectra. However, the difference with the ones based on the velocity and energy ratio remains often restricted. The degree of cement hydration, solid percolation and formation of hydration products is clearly related to the ultrasonic measurements. Only the pore space percolation does not relate to the measurements at all.

1. Introduction

The potential and advantages of ultrasonic measurements to monitor the setting process of mortar or concrete have been elaborated by the author in previous publications [1–3] and by other researchers such as Reinhardt and Grosse [4], Voigt et al. [5] and Lee et al. [6]. The change in velocity, amplitude and frequency content of compression waves (p-waves) sent through a hardening specimen indicate the change in stiffness of the sample. The corresponding microstructure development in the cement paste fraction fundamentally causes this change from fluid to solid, but is however still difficult to be monitored experimentally. While the hydrated microstructure at a certain age can be investigated in two dimensions using scanning electron microscopy (SEM), the three-dimensional microstructure change from viscous suspension to solid is difficult to observe with traditional laboratory equipment. The microstructure development of the cement paste includes the formation of hydration products (solid phase) and pore structure (pore phase). The fraction of solid particles, connected from one side to the other (solid percolation) is the parameter which is most directly related to the setting [7] and can best be measured in three dimensions. Rapoport et al. [8] suggested that also the pore space depercolation might influence the ultrasonic measurements during setting. Pore space depercolation occurs when no complete pathway of water from one side of the specimen to the other exists anymore. Even after solid percolation, the ultrasonic measurements are still affected by the microstructure as the hydration products fill up the pore space and thereby increase the elastic moduli.

Computer simulation models offer an alternative for laboratory experiments to study the microstructure changes in fresh cement paste during setting and also enable three-dimensional observations. The relation between early-age microstructure development and ultrasonic velocity change has been investigated by Ye [7] with computer simulations for ordinary Portland cement (OPC). The largest velocity increase occurred during setting when the cement hydrates start to percolate and form complete pathways of connected particles for the ultrasonic pulse wave. The study was however restricted to the ultrasonic wave velocity and blended cement types were not investigated.

1.1. Objectives

In this research, the relation between ultrasonic measurements and fundamental changes in the cement paste is investigated for several mixtures with ordinary Portland cement (OPC) and

* Corresponding author. Tel.: +32 9 264 55 22; fax: +32 9 264 58 45.
E-mail address: Nele.DeBelie@UGent.be (N.D. Belie).

0958-9465/$ - see front matter © 2011 Elsevier Ltd. All rights reserved.
doi:10.1016/j.cemconcomp.2011.03.004

additions such as fly ash (FA) and blast-furnace slag (BFS). To simulate the microstructure changes, CEMHYD3D was selected as computer model. The objectives of this study can be divided into two parts. First, the CEMHYD3D model was extended to include considerations of pH of the pore solution, and to be applicable to cement blended with BFS and FA. The original version will be indicated as CEMHYD3D v.3, the adjusted version as v.3n. The adjustments were validated by comparison with results of isothermal calorimetry, electron microscopy and thermal analysis. Secondly, the measured ultrasonic velocity, energy and frequency spectrum were related to volume fraction (connected) solid phase and other microstructure parameters with the support of the extended CEMHYD3D model. For this purpose, a multi-variate and multi-way regression was performed between the ultrasonic results and the microstructure parameters.

1.2. Simulating microstructure development

Several cement microstructure models have already been developed, which can mainly be divided into vector (e.g. HYMOSTRUC [9]) and discrete models (e.g. CEMHYD3D [10]). Details about these models can be found in the work of van Breugel [11] and Bentz [10].

CEMHYD3D offers the possibility to simulate the hydration of blended cement, which is necessary for this study. Moreover, the open-source code allows the user to adjust the model if necessary. In CEMHYD3D, cement particles are represented by a spherical collection of voxels (1 μm^3) to which mineralogical phases are assigned according to the clinker distribution on a SEM image. The autocorrelation function is calculated which expresses the probability that the neighbouring pixels will be of the same phase. This spatial correlation is then applied in three dimensions. The chemical reactions between these pixels are simulated by cellular automaton (CA) rules, applied to the pixels of the microstructure forming potential reaction sites for a given iteration [12].

1.3. Relating ultrasonic measurements to the microstructure development

During ultrasonic measurements, a large amount of data can be collected. For different mortar and concrete samples, the velocity, energy and frequency content of ultrasonic waves sent through this hardening sample are recorded in function of time. The analysis of such data sets with more than one statistical variable can be performed with multi-variate data-analysis techniques. In a previous publication, Robeyst et al. [1] related the change of the frequency spectra to the setting behaviour by multi-way data-analysis, a specialised branch of multi-variate statistics extending the standard methods for two-way data to multi-way data.

In this study, the relation between the ultrasonic results and microstructure parameters is investigated by multi-way regression. Comparable to normal linear regression, a relation between predictor (ultrasonic results) and response data (microstructure parameter) is determined. The method of multi-variate and multi-way regression analysis was chosen in order to predict the microstructure parameters based on as much ultrasonic measurement data as possible in their original two-dimensional (velocity/energy in function of sample and concrete age) or three-dimensional structure (frequency content in function of concrete sample, frequency and concrete age). Moreover, multi-way analysis allows comparing the results of all samples simultaneously and detects differences and similarities based on the variation of the entire dataset.

2. Materials and methods

2.1. Mixtures

The chemical and physical details of the OPC (CEM I 52.5 N), BFS and FA are given in Table 1. Cement paste mixtures were used to study the heat release during hydration, both by experiments and simulations. A slag-to-binder (s/b) ratio of successively 0, 0.30, 0.50, 0.70 and 0.85 and a water-to-binder (w/b) ratio of 0.5 was used for the BFS mixtures. The compositions with FA had a w/b ratio of 0.4 and a fly-ash-to-binder (f/b) ratio of successively 0, 0.35, 0.50 and 0.67.

For the ultrasonic measurements, concrete mixtures were made with a w/b ratio of 0.5 and 0.4 for BFS and FA mixtures, respectively (Table 2). However, since only cement paste can be modelled with CEMHYD3D, the corresponding simulations were performed on the cement paste fraction of these mixtures. According to Eq. (1), which is based on the principles of the MBE method (Mortier de béton équivalent) [13], the w/b ratio of this cement paste fraction was calculated to be 0.45 and 0.35 for the BFS and FA mixtures respectively.

$$\Delta f_{water} = f_{sand} \cdot A_{sand} - f_{gravel,1} \cdot A_{gravel,1} - f_{gravel,2} \cdot A_{gravel,2} \quad (1)$$

f and Δf are respectively the mass fraction and the change in mass fraction of the indicated component. The absorption coefficients were 0.009 for 0/4 sand (A_{sand}), 0.015 for 2/8 gravel ($A_{gravel,\ 1}$) and 0.014 for 8/16 gravel ($A_{gravel,\ 2}$) as determined according to EN 1097-6. Jones' multi-phase theory [14] states that the transit time of an ultrasonic wave in multi-phase media equals the sum of the transit times in each phase. The velocity in concrete and in the corresponding cement paste fraction would thus be directly related. However, the presence of sand and gravel in concrete already causes a different hydration and setting behaviour compared to cement paste due to the thermal capacity, surface area and interfacial transition zone of the aggregates. Moreover, although the increase in wave velocity and energy is mainly caused by the monitored setting, also other factors such as air bubble migration, internal settling and thixotropy affect the velocity change in time [3]. This can also cause differences between ultrasonic velocity measurements on cement paste, mortar and concrete. Finally, for the measurements of ultrasonic energy and frequency content changes,

Table 1
Chemical composition (%), mineralogical composition according to the Bogue calculations (%), specific gravity (–) and Blaine specific surface area (m^2/kg) of the cement, blast-furnace slag and fly ash.

Binder		CEM I 52.5 N[a,b]	BFS	FA[b]
Chemical composition				
CaO	C	62.21	41.70	3.21
SiO_2	S	18.84	34.09	53.58
Al_2O_3	A	5.39	10.19	26.49
Fe_2O_3	F	3.79	0.48	7.01
MgO	M	0.86	7.62	2.08
SO_3		3.06	1.71	–
CO_2		0.72	0.25	–
Na_2O		0.41	0.29	0.52
K_2O		0.77	0.37	3.58
Cl^-		0.04	0.013	–
LOI		1.89	0.48	3.90
Mineralogical composition				
C_3S		66.8	–	–
C_2S		4.2	–	–
C_3A		4.9	–	–
C_4AF		14.2	–	–
Specific gravity		3.12	2.80	2.55
Blaine		390	400	275

[a] Nomenclature according to EN 197-1.
[b] Mean chemical composition of two batches.

Table 2
Specifications of the studied concrete mixtures with CEM I 52.5 N (EN 197-1): addition-to-binder ratio (a/b), water-to-binder ratio (w/b), composition (kg/m^3) and admixture (ml/100 kg cement), slump (mm), air content (vol.%), compressive strength (MPa) and setting times (h).

Sample number	a/b	w/b	Composition						Adm.	Slump[b]	Air content[b]	Strength[b]		Setting times[b]	
			Cem.	BFS	FA	Sand 0/4	Grav 2/8	Grav 8/16	SP[a]			7 days	28 days	Initial	Final
Series 1: BFS															
1, 2, 3	0	0.5	350	–	–	791	425	618	–	130	2.5	41	51	5.66	8.12
4	0.15	0.5	297	52	–	790	425	617	–	60	2.7	40	52	5.86	8.27
5	0.30	0.5	245	105	–	789	424	617	–	120	2.9	35	49	6.07	8.46
6, 7	0.50	0.5	174	174	–	788	423	616	–	80	2.1	32	44	6.35	8.70
8, 9, 10	0.70	0.5	104	244	–	787	423	615	–	70	1.9	24	38	7.90	13.1
11, 12	0.85	0.5	52	295	–	785	422	614	–	50	1.4	18	30	8.80	18.6
Series 2: FA															
13, 14	0	0.4	400	–	–	686	451	694	65	40	3.1	55	62	5.66	8.12
15, 16	0.35	0.4	260	–	140	668	437	678	100	40	2.3	47	56	6.51	9.29
17, 18	0.50	0.4	200	–	200	660	432	668	100	65	2.0	28	39	7.67	11.7
19, 20	0.67	0.4	132	–	268	652	427	660	110	35	2.0	17	24	8.63	12.3

[a] Superplasticizer: carboxylic ether polymer with long side chains (con. 35%).
[b] The repeatability r of the slump is 16 mm (EN 12350-2) and of the air content is 0.4% (EN 12350-7). The repeatability r of the strength, expressed as percentage of the mean, is 9.0% (EN 12390-3). The repeatability r of the initial and final setting time, expressed as percentage of the mean, is respectively 23% and 16% (ASTM C403).

scattering and attenuation by aggregates causes additional differences between experiments on cement, mortar and concrete samples. Considering these limitations, the experimental results using concrete and the simulation with cement paste must thus be compared carefully.

SEM images were taken of cement paste samples ($w/b = 0.5$) with an s/b ratio of 0 and 0.85. In addition, the BSE image of a sample with an f/b ratio of 0.50, taken by Baert [15] was also considered.

The change of CH content during hydration was determined with DTA-TGA by Gruyaert et al. [16] on cement paste with BFS ($w/b = 0.5$, $s/b = 0$, 0.50 and 0.85) and by Baert [15] on cement paste with FA ($w/b = 0.4$, $s/b = 0$, 0.50 and 0.67). The details of this method can be found in the mentioned references.

2.2. Isothermal measurements

Isothermal calorimetric tests were performed on the cement paste mixtures. Each chamber of the heat conduction calorimeter (TAM air) is constructed in twin configuration with the test sample on one side and an inert reference on the other. The twin configuration allows the comparison between the heat flow of the active sample and the reference, which enhances the stability and limits the noise [17]. Each sample ampoule contained 15 g cement paste and all tests were conducted at a temperature of 20 °C.

2.3. Ultrasonic measurements

The ultrasonic measurements were performed with the through-transmission FreshCon system, developed at Stuttgart University [18]. The setup used for this study has already been described in detail previously [3]. With this technique, the velocity, energy and frequency spectra of ultrasonic compression waves (p-waves) sent through the fresh mortar or concrete sample are measured.

The ultrasonic energy (E) was determined by numerical integration of the squared amplitude values following the onset time of the received signal. To minimise the energy loss due to divergence and reflection at the contact interfaces, this value was then divided by the reference energy (E_{ref}) measured on the container filled with water. Therefore, the energy ratio (E/E_{ref}) will be used as quantity to describe setting instead of the absolute value. The frequency spectrum was determined as the fast Fourier transform (FFT) of the received signal.

During the setting and hardening process, the sample container was sealed with plastic tape to limit concrete shrinkage resulting in decoupling of the sample and the container walls. All ultrasonic experiments were performed at an ambient temperature of 20 °C ± 2 °C.

2.4. SEM images

For each tested mixture, cylindrical moulds were filled with cement paste and rotated at a speed of 5 rotations/min for 24 h to prevent bleeding. Afterwards, they were cured in water at a temperature of 20 ± 2 °C. At the age of 2 days, the cylinders were ground into small pieces and the hydration of the specimen was stopped by submersion in methanol during 1 week. To minimise the possible influence of methanol, the samples were then dried in a desiccator with silica gel for another week prior to testing, as indicated by Pane and Hansen [19] and Baert [15]. Although the methanol treatment is under discussion, Baert [15] demonstrated that no significant change in measurable amount of CH as determined by thermal analysis is introduced.

The small pieces of these samples were placed into a mould and impregnated with epoxy resin under vacuum. A specimen was cut from these samples and subsequently polished with sandpaper 300, 500, 1200 and 4000 grit, followed by 6, 3, 1 and 0.25 μm diamond paste, each step during 120 s. The prepared samples were placed into the environmental scanning electron microscope (ESEM) chamber with 1 Torr pressure and accelerating voltage of the beamer of 20 kV. 15 backscattered electron (BSE) images were taken at random locations which were segmented into unhydrated cement, slag or fly ash and hydrated phases based on greyscale thresholds. Dense phases such as ferrite appear as bright constituents on the BSE image, while porosity appears as black [20]. Since the grey level of BFS overlaps with these of unhydrated clinker (especially C_3A) and CH, the BFS grains were also manually selected from the image, based on their characteristic angular appearance.

2.5. Simulations with CEMHYD3D

2.5.1. Constructing the initial cement paste microstructure

The SEM image for the distribution of the clinker phases was taken according to the method proposed by Stutzman [20]. The prepared sample was placed in the ESEM chamber as described above and five BSE images were taken. These BSE images were segmented into cement phases based on greyscale thresholds. However, the segmentation is ambiguous since the grey levels of for instance C_2S and C_3A generally overlap. Therefore, the results of the BSE

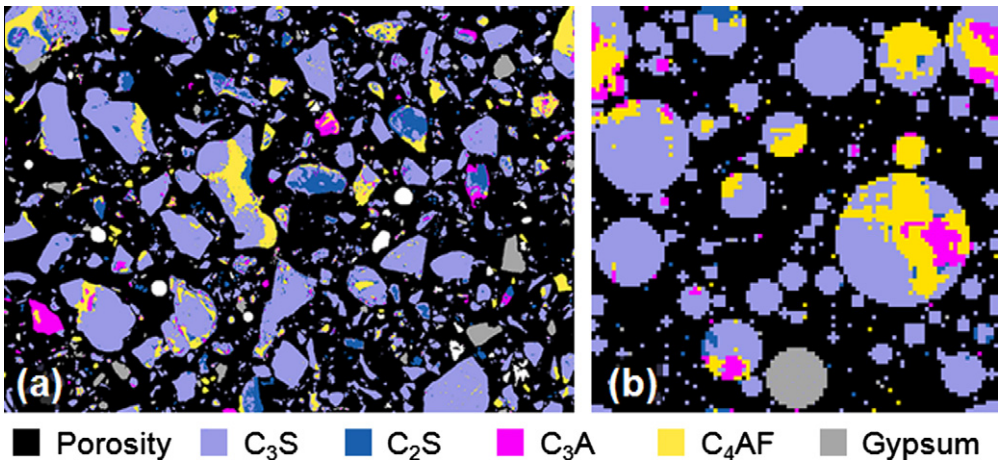

Fig. 1. (a) Final segmentation of the OPC (CEM I 52.5 N) blended in epoxy resin, based on the BSE image and X-ray mappings and (b) 2D-slice of corresponding initial microstructure in CEMHYD3D.

image were completed with X-ray spectroscopy mappings, collected for the elements Ca, Si, Al, Fe, K, S, Na and Mg. The decision tree of Bentz et al. [21] was applied to segment the cement powder into phases based on the X-ray mappings. For the final segmentation, the BSE image and the X-ray mappings were combined and the result is shown in Fig. 1a. During the stereological analysis of this image, the area and perimeter fractions of the clinker phases as well as their spatial correlation is calculated, as described by Bentz [22]. Fig. 1b shows a 2D-slice of the initial microstructure of the virtual cement paste (100% OPC, $w/b = 0.5$).

2.5.2. BFS and FA particles

In CEMHYD3D v.3, the reaction of BFS has been implemented preliminary. The slag particles are placed in the first step of the procedure as mono-phase particles. Their characteristics (molar mass, molar volume, specific gravity, Ca/Si molar ratio of initial slag and slag hydration product) are saved in a separate input file that is addressed during the execution of the simulation. The characteristics of the BFS used in this study were determined based on the chemical analysis (Table 1) and the examples given by Bentz [12].

Bentz and Remond [23] also extended the model with the incorporation of FA. Similar to BFS particles, FA grains are placed in the first step of the procedure as mono-phase particles. However, FA is considered as a mixture of several phases. In this study, the fly ash contained 24% silica (S), 38% aluminosilicate glass (ASG) and 38% inert material [15]. In an additional procedure step of CEMHYD3D v.3, these phases are randomly distributed amongst the FA particles, while the continued procedure remains the same.

2.5.3. Calibration cycle-to-time factor

Each cycle c of the CA model corresponds to some unit of ageing time t in the material [10] according to Eq. (2). In this equation, there is no constant representing the dormant period. Instead, the dormant period is simulated by making the early-time dissolution probabilities of the cement clinker phases proportional to the square of the amount of formed C—S—H without exceeding the base dissolution probabilities ([24], p. 33).

$$t = \beta \cdot c^2 \tag{2}$$

A good fit between the dormant period indicated by the simulated and experimental heat production rate was obtained when the calibration factor β was set to 0.00035, which corresponds exactly with the value of Bentz [12] and Chen et al. [25]. For all further simulations, this value is applied.

2.5.4. Influence of pH on the cement hydration

Higher pH of the pore water tends to accelerate the hydration reactions of the cement phases. In the source code of CEMHYD3D v.3, higher pH results in higher reactivity of the clinker minerals via the pH factor variable according to Eq. (3) [12]. The initial dissolution probability P^0_{clinker} varies for the different clinker phases.

$$P_{\text{clinker}} = P^0_{\text{clinker}} \cdot \frac{1}{1 + \text{pH factor}} \tag{3}$$

The pH factor is defined as a stepwise function of the pH as shown in Fig. 2. During the first days after mixing, the pH of the pore solution can change rapidly. To better capture these pH changes, the step size of pH factor was reduced (Fig. 2). CEMHYD3D v.3 with this small adjustment will be indicated as CEMHYD3D v.3*. The actual improvements to simulate the reaction of BFS and FA will be described in Section 3 and are noted as CEMHYD3D v.3n.

2.5.5. Microstructure parameters

The solid percolation, pore space percolation, degree of cement hydration, degree of total binder hydration and formation of hydration products will be related to the ultrasonic measurements. The hydration products CH and monosulphate (AFm) share a Young's modulus of 42.3 GPa [26] and will therefore be referred to as hydration products of type I. Calcium silicate hydrates (C—S—H), ettringite (Aft) and hydrogarnet (C_3AH_6) share an estimated modulus of 22.4 GPa [26] and will be called type II hydration products.

2.6. Multi-way analysis

2.6.1. Applied multi-way regression models

Multi-way analysis was performed to relate the change in ultrasonic parameters, compiled in the predictor matrix **X** (velocity or energy) or three-dimensional array $\underline{\mathbf{X}}$ (spectra), to the changing microstructure parameters from CEMHYD3D v.3n, compiled in the response matrix **Y**. PLS and N-PLS are used for the two- and three-dimensional datasets respectively. PLS finds a linear regression model by projecting **X** and **Y** to a new variable space. The number of variables is hereby reduced to a set of r so-called latent variables (LV's) which contain all the relevant information. The technique for multi-way regression (N-PLS) is basically the same as the PLS regression described above, but with use of the multi-way structure of the predictor data $\underline{\mathbf{X}}$ [27]. More information about PLS and N-PLS can be found in the work of Smilde et al. [28]. The

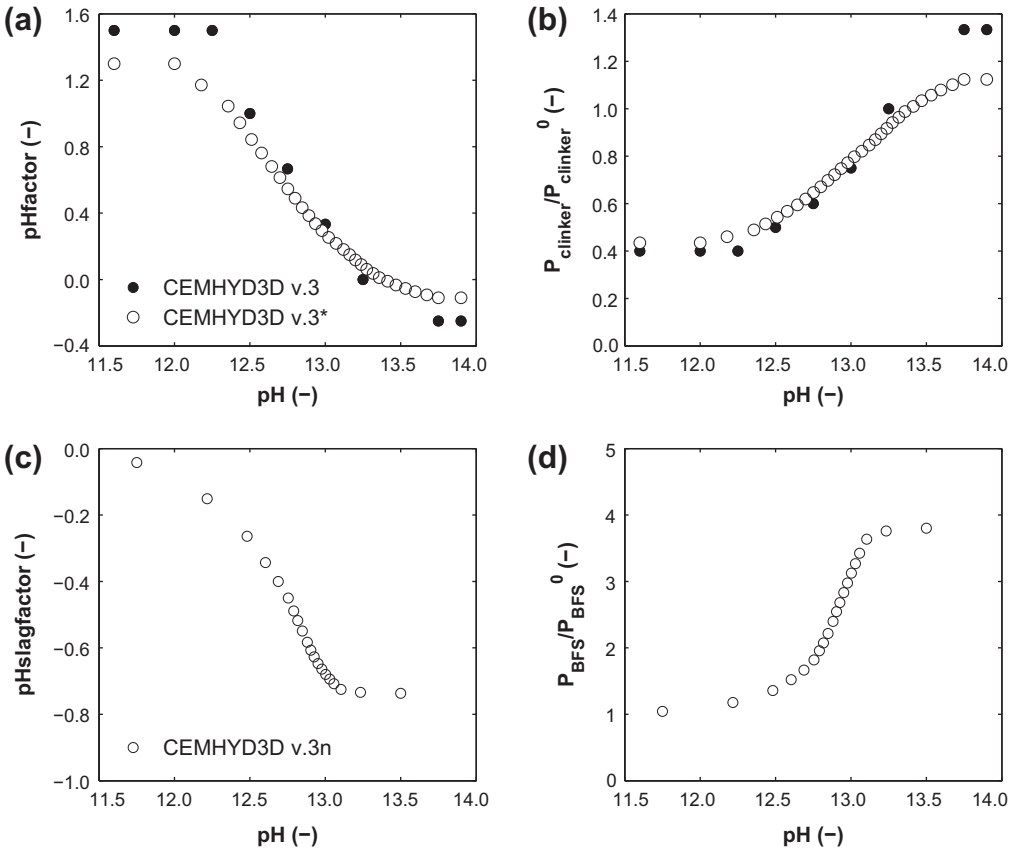

Fig. 2. (a) The original (v.3) and adjusted (v.3∗) stepwise pH factor vs. pH and (b) the corresponding change in the dissolution probability; (c) the introduced (v.3n) stepwise pH slag factor vs. pH and (d) the corresponding change in the dissolution probability.

calculations of the models were performed with the PLS_Toolbox Version 3.5 for use with MATLAB™ designed by Wise et al. [29].

2.6.2. Data arrangement for predicting microstructure development

Three-way $\underline{\underline{\boldsymbol{X}}}$ array The ultrasonic spectral data were arranged in a three-way array: 20 samples × 400 frequencies × 189 ages. The frequencies ranged from 0 to 245 kHz in steps of 610 Hz. The concrete ages ranged from 0.25 to 47.25 h in steps of 0.25 h.

Two-way $\boldsymbol{X}$ matrix. The measurements of the velocity and energy ratio were arranged into two matrices of 20 samples × 189 ages.

Two-way $\boldsymbol{Y}$ matrix. The six microstructure parameters (degree of cement hydration, degree of binder hydration, solid percolation, pore space percolation, hydration products I and hydration products II) were arranged into six two-way matrices of 20 samples × 189 ages.

2.6.3. Model validation

To select the optimum r (number of LV's), the errors between the predicted and the actual values were calculated. The root-mean-square error of calibration (RMSEC) for a variable is defined by the following equation [29]:

$$\mathrm{RMSEC} = \sqrt{\frac{\sum_{j=1}^{m}\sum_{i=1}^{n}(\hat{y}_{ij} - y_{ij})^2}{m \cdot n}} \tag{4}$$

where $\hat{y}_{ij}$ is the value of the predicted variable when all samples are included in the model formulation, m the number of time steps and n the number of calibration samples. The RMSEC is a measure of how well the model fits the data.

The model's ability to predict new samples is investigated by performing a cross-validation. The calculation is analogous, except $\hat{y}_{ij}$ is the prediction for sample i if sample i is not included in the model formulation. Two methods were used to cross-validate the model.

In the leave-one-out (loo) method, every sample was successively excluded. The model constructed by this reduced dataset as calibration set was then used to predict the excluded element and to calculate the R^2_{loo} as given by the following equation [30]:

$$R^2_{i,\mathrm{loo}} = 1 - \frac{\sum_{j=1}^{m}(\hat{y}_{ij,\mathrm{loo}} - y_{ij})^2}{\sum_{j=1}^{m}(y_{ij} - \bar{y}_i)^2} \tag{5}$$

where $\hat{y}_{ij,\mathrm{loo}}$ is the value of the predicted variable when sample i is not included in the model formulation, $\bar{y}_i$ is the average of y_{ij} over time and m is the number of time steps. The R^2 values given in the results section are averaged over all samples. Values of R^2 close to 1 indicate a good prediction while those close to 0 or even negative indicate a poor regression.

In addition to the leave-one-out method, the dataset was also split into two parts: a calibration and a validation set. The calibration set consisted of all samples of series 1 (BFS) and the results of series 2 (FA) were used as validation set. The R^2_{split} for a variable was calculated as shown in the following equation:

$$R^2_{i,\mathrm{split}} = 1 - \frac{\sum_{j=1}^{m}(\hat{y}_{ij,\mathrm{split}} - y_{ij})^2}{\sum_{j=1}^{m}(y_{ij} - \bar{y}_i)^2} \tag{6}$$

where $\hat{y}_{ij,\mathrm{split}}$ is the value of the predicted variable of validation sample i and m is the number of time steps.

The cross-validation according to the leave-one-out method indicates how well the model can predict results of samples similar to those of the calibration data set. The split-half cross-validation, on the other hand, investigates the ability of the model to predict the results of samples that differ from the calibration set.

3. Adaptation and validation of the hydration simulation of blended mixtures

As mentioned above, CEMHYD3D v.3 with the small adjustment of the *pH factor* is indicated as CEMHYD3D v.3*. The final version with the further improvements to simulate the reaction of BFS and FA will be indicated as CEMHYD3D v.3n.

3.1. Adaptation of the reaction of BFS in CEMHYD3D v.3*

The adaptation of the BFS reaction was made based on the mixture with a *s*/*b* ratio of 0.50. The heat production of this cement paste is shown in Fig. 3 as simulated with CEMHYD3D v.3*, which assumes that BFS reacts with CH to produce C—S—H with a lower Ca/Si ratio than the conventional C—S—H. The activation of the slag reaction by high hydroxyl concentrations in the pore solution is not completely considered. The *pH factor*, defined for clinker phases, is currently also applied on BFS. However, the reaction of BFS is more influenced by the pH of the pore solution than the clinker phases so the use of the pH factor might not serve for the BFS reaction. Therefore, a separate pH slag factor was introduced, determining the dissolution probability of the slag particles by analogy with the pH factor for the clinker phases, as shown in the following equation:

$$P_{BFS} = P^0_{BFS} \cdot \frac{1}{1 + \text{pH slag factor}} \tag{7}$$

This pH slag factor in function of pH was determined by trial and error to achieve the best fit (least-square method) between the simulated heat production and the measurements with the isothermal calorimeter for the mixture with 50% BFS. The final pH slag factor is shown in Fig. 2c. The new version of the source code will be indicated as CEMHYD3D v.3n.

This study is restricted to the use of one type of BFS. In further research, the *pH slag factor* can be made dependent on the chemical composition of the BFS. Chen et al. [25] suggested to use the NBO/T ratio which is the amount non-bridging oxygen per tetrahedron [31] as an indicator of the slag reactivity. A low NBO/T ratio corresponds to a high degree of polymerisation and thus low activity of the silicate glass. The NBO/T ratio of BFS can be calculated based on the oxide fractions from a chemical analysis [32]. For the BFS used in this study, the NBO/T ratio amounted to 2.194 which is rather high, since the NBO/T values in the extensive research of Wolter et al. [33] ranged from 1.5 to 2.5.

However, the *pH slag factor* in CEMHYD3D v.3n suffices for this study, concentrating on monitoring the setting and microstructure development of these BFS mixtures with ultrasonic waves.

3.2. Validation of the reaction of BFS in CEMHYD3D v.3n

The first validation consisted of a comparison between measured and simulated results of the other mixtures (*s*/*b* = 0, 0.15, 0.30, 0.70 and 0.85). The simulated heat production during hydration is presented in Fig. 4 for all the BFS pastes. The second peak, attributed to the massive hydration of C_3S, was less broad and occurred approximately 2 h earlier compared to the experimental results. For the mixtures with BFS replacement, the third peak was initially steeper than the one of the measured heat production rate, but less high and decreased more gradually. This peak is generally attributed to the BFS reaction which is activated by the CH produced during C_3S hydration.

In CEMHYD3D, however, BFS reacts from the beginning, but at a slow rate. This reaction is accelerated by the increasing pH of the pore solution via the *pH factor* in CEMHYD3D v.3* or via the *pH slag factor* in CEMHYD3D v.3n. A discontinuity occurred in the pH change after approximately 24 h for all the BFS mixtures. When all of the gypsum is consumed and the ettringite becomes unstable, the pore composition module switches from an equilibrium between CH, gypsum and pore solution to one between CH and pore solution. The sulphate concentration is set to zero and more hydroxyl ions are generated to maintain electroneutrality with the cations (e.g. K^+, Na^+) in the pore solution. This step change produced by CEMHYD3D is an approximation of the more gradual rise that occurs in pH in a real system during this time and explains the rather sudden increase in the heat production rate corresponding with the third hydration peak.

The step change in the pH curve also occurred for the mixture without BFS replacement, but after 72 h and to a lesser degree. The simulated cumulative heat production fits the measured one well, indicating that the model is indeed improved by introducing the pH slag factor to stimulate the slag reaction at higher pH.

To obtain an additional validation of CEMHYD3D v.3n model, the results of the simulations were compared to BSE images and DTA-TGA measurements. A quantitative comparison between the CEMHYD3D v.3n output and the BSE images was established by counting the pixels of the different phases, as summarised in Table 3. The largest difference between both is noticed for the C—S—H and porosity counts. The grey level threshold between these two

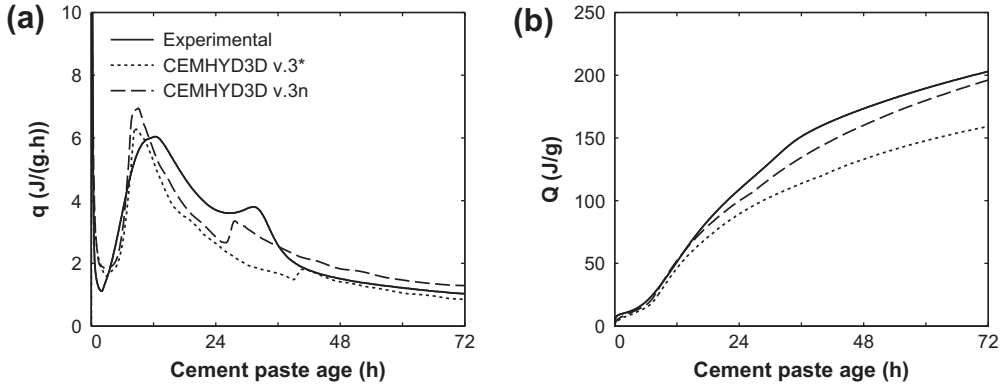

Fig. 3. (a) Heat production rate *q* (*J*/*h* per g binder) and (b) cumulative heat production *Q* (*J* per *g* binder) for cement paste (*w*/*b* = 0.50) with 50% OPC and 50% BFS, experimentally determined and simulated with CEMHYD3D (v.3* and v.3n) under isothermal conditions (20 °C).

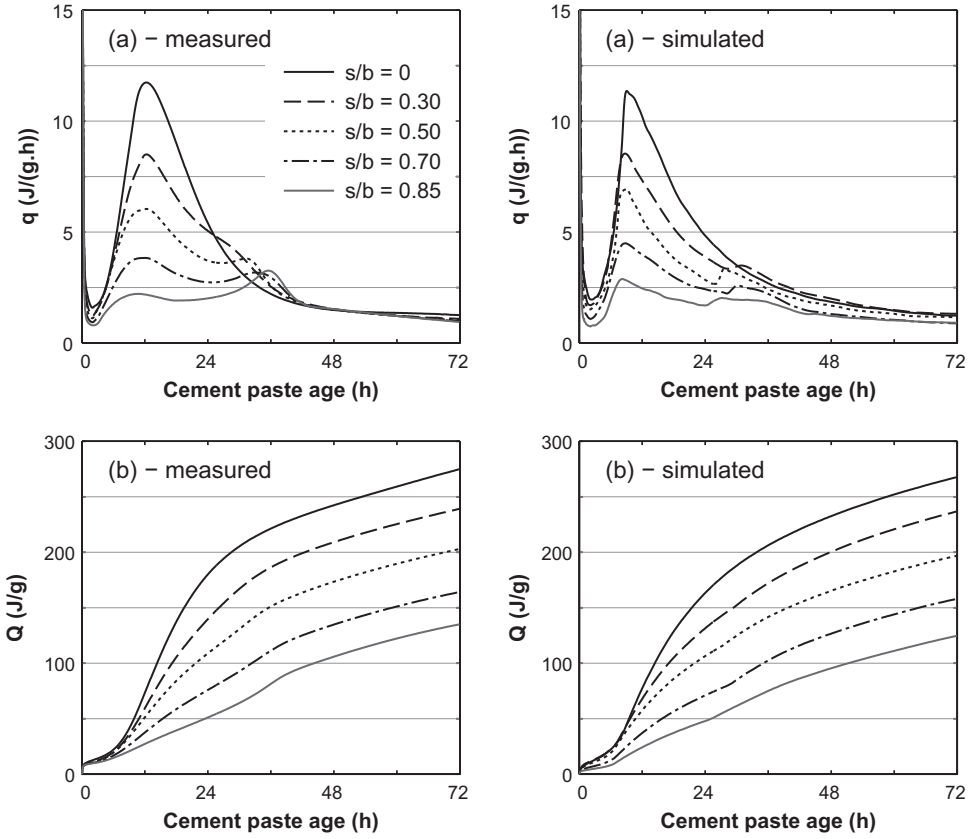

Fig. 4. (a) Heat production rate q (J/h per g binder) and (b) cumulative heat production Q (J per g binder) for cement paste ($w/b = 0.50$) with an increasing percentage of OPC replaced by BFS, experimentally determined (left) and simulated with CEMHYD3D v.3n (right) under isothermal conditions (20 °C).

Table 3
Comparison between the phase fractions (%) at 2 days determined with the BSE image ($n = 15$, standard deviation indicated) and determined with CEMHYD3D v.3n. The results of the fly ash mixture were obtained by Baert [15].

Phase	Mixture					
	0% BFS		85% BFS		50% FA[a]	
	BSE images	CEMHYD3D	BSE images	CEMHYD3D	BSE images	CEMHYD3D
Pore	29.5 ± 6.8	35.6	38.4 ± 3.4	40.8	36.0 ± 1.8	40.0
Unhydrated clinker	17.8 ± 3.3	23.1	4.1 ± 2.6	2.5	36.0 ± 1.8[b]	10.8
Unhydrated BFS/FA	–	–	33.5 ± 3.2	35.6		26.8
C—S—H	43.7 ± 7.5	33.3	22.5 ± 2.0	19.8	24.5 ± 3.2	17.2
CH	8.8 ± 3.0	9.29	1.5 ± 1.8	1.6	4.5 ± 0.5	5.3

[a] No image was taken by Baert [15] at 2 days; an interpolation between 1 and 3 days was made.
[b] No distinction between unhydrated clinker and FA was made by Baert [15].

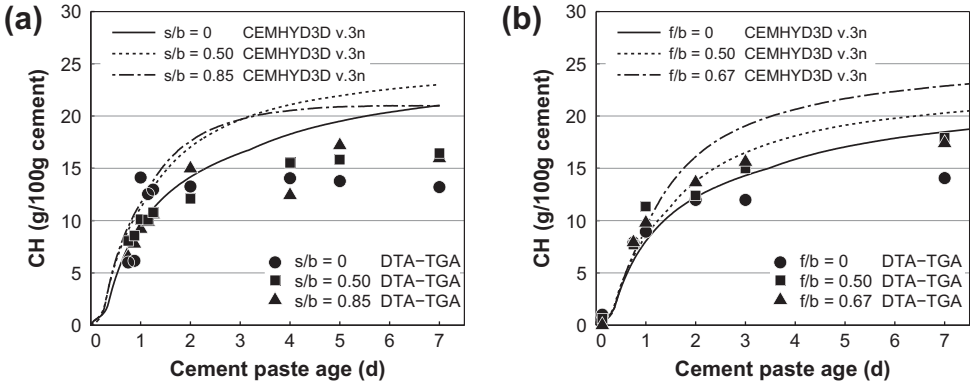

Fig. 5. Comparison of the change of CH content during hydration as determined with DTA-TGA and as simulated with CEMHYD3D v.3n for (a) cement pastes ($w/b = 0.5$) with different replacement levels of BFS [16] and (b) cement pastes ($w/b = 0.4$) with different replacement levels of FA [15].

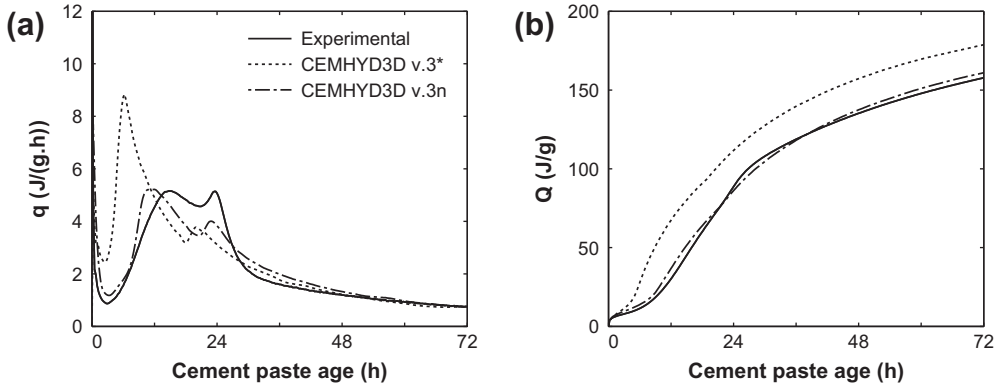

Fig. 6. (a) Heat production rate q (J/h per g binder) and (b) cumulative heat production Q (J per g binder) for cement paste ($w/b = 0.40$) with 50% OPC and 50% FA, experimentally determined and simulated with CEMHYD3D (v.3* and v.3n) under isothermal conditions (20 °C).

fractions on a BSE image was however difficult to determine unambiguously, hence more variation on these fractions was expected. A good general correspondence between the CEMHYD3D v.3n output and the BSE images is however noticed.

The change of CH content during hydration as determined with DTA-TGA by Gruyaert et al. [16] is given in Fig. 5a. The amount of CH present in a cement paste sample can be used as an indicator for the progressing hydration of both cement clinker (CH production) and BFS or FA (CH consumption). These results are compared to the CH change simulated by CEMHYD3D v.3n. For the mixtures with an s/b ratio of 0.50 and 0.85, the simulated CH content was clearly higher than the one measured with DTA-TGA, especially after 2 days. This difference was much less for the OPC mixture ($s/b = 0$). The consumption of CH by the reaction of BFS might need improvement in the CEMHYD3D v.3n model. On the other hand, thermal methods are considered to give low CH results due to the presence of amorphous CH [34] or because the CH is partly adsorbed on the C—S—H [35] or present as interlayer material [36]. Moreover, the simulations of CEMHYD3D v.3n agreed well with the BSE images.

3.3. Adaptation of the reaction of FA in CEMHYD3D v.3*

Similar to BFS, the *pH factor*, defined for clinker phases, is currently also applied on the S and ASG phases of the FA. Contrary to the BFS reaction, this pH factor might suffice for the early-age simulations, since the pozzolanic reaction of FA is slow and thus

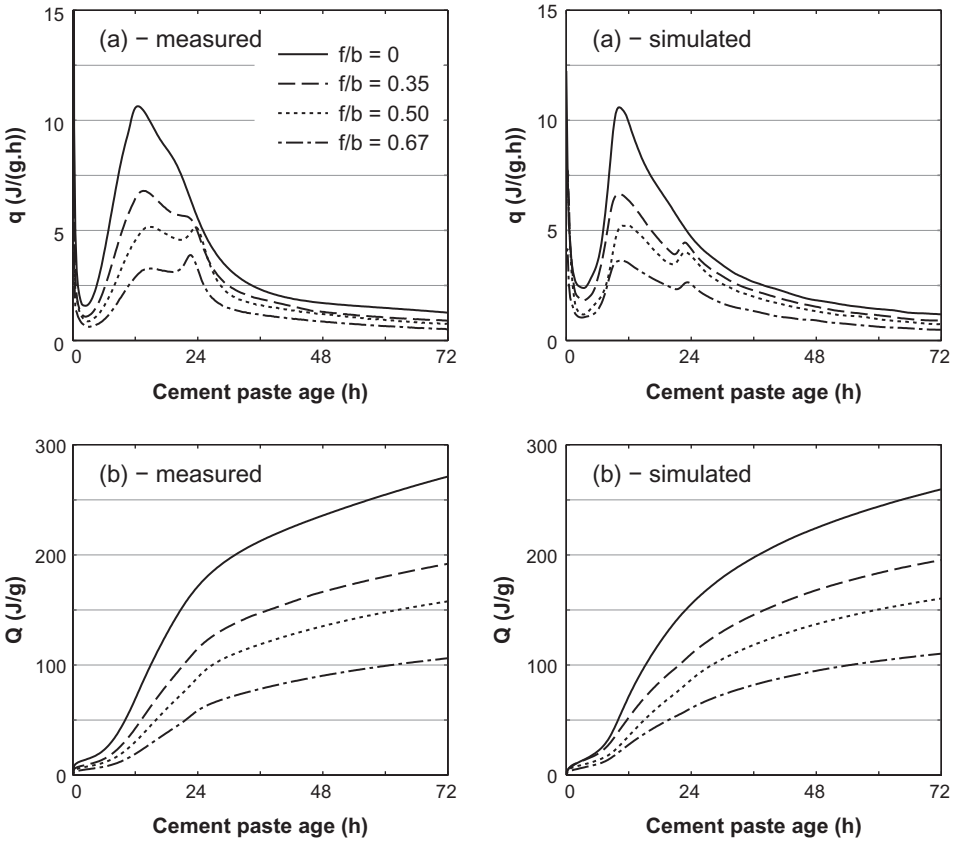

Fig. 7. (a) Heat production rate q (J/h per g binder) and (b) cumulative heat production Q (J per g binder) for cement paste ($w/b = 0.40$) with an increasing percentage of OPC replaced by FA, experimentally determined (left) and simulated with CEMHYD3D v.3n (right) under isothermal conditions (20 °C).

Table 4
Diagnostics of the N-PLS models between measured frequency spectra and simulated microstructure parameters: RMSEC (%), R^2_{loo} (–) and R^2_{split} (–).

Number of LV's		1	2	3	4	5	6	7	8	9	10
Degree of hydration (cement)	RMSEC	1.83	1.19	0.98	0.69	0.54	0.42	0.35	0.3	0.27	0.23
	R^2_{loo}	0.98	**0.99**	0.99	0.99	0.99	0.99	0.99	0.99	0.99	0.99
	R^2_{split}	0.91	**0.91**	0.90	0.88	0.87	0.89	0.90	0.90	0.90	0.90
Degree of hydration (total binder)	RMSEC	2.10	1.38	1.09	0.94	0.75	0.66	0.55	0.51	0.48	0.46
	R^2_{loo}	0.87	**0.93**	0.92	0.92	0.90	0.89	0.87	0.90	0.90	0.90
	R^2_{split}	0.05	**0.63**	0.53	0.57	0.39	0.39	0.26	0.15	0.08	−0.23
Solid percolation	RMSEC	8.19	4.74	3.53	2.58	2.17	1.71	1.57	1.24	1.06	0.97
	R^2_{loo}	0.71	**0.93**	0.94	0.97	0.98	0.98	0.98	0.99	0.99	0.99
	R^2_{split}	0.69	**0.86**	0.84	0.66	0.61	0.44	0.45	0.40	0.40	0.29
Pore space percolation	RMSEC	0.61	0.33	0.22	0.17	0.12	0.1	0.07	0.06	0.05	0.04
	R^2_{loo}	−0.36	−0.67	−1.45	−1.19	−0.72	−0.69	−0.48	−0.48	−0.33	−0.31
	R^2_{split}	−262	−84.7	−39.7	−50.1	−26.0	−31.1	−32.2	−34.0	−34.8	−34.8
Hydration products I formed (CH, AFm)	RMSEC	0.47	0.33	0.31	0.24	0.19	0.16	0.14	0.13	0.12	0.11
	R^2_{loo}	0.80	**0.82**	0.69	0.52	0.35	0.27	0.28	0.32	0.40	0.39
	R^2_{split}	0.21	**0.88**	0.88	0.69	0.63	0.58	0.60	0.56	0.46	0.24
Hydration products II formed (C—S—H,...)	RMSEC	1.31	0.92	0.67	0.57	0.48	0.42	0.36	0.33	0.31	0.30
	R^2_{loo}	0.89	**0.93**	0.91	0.92	0.92	0.9	0.89	0.89	0.90	0.90
	R^2_{split}	0.09	**0.82**	0.80	0.76	0.70	0.67	0.61	0.54	0.51	0.35

restricted during the first 3 days after mixing. Analogously to the study of the BFS reaction, the adjustments were made based on the mixture with f/b = 0.50 of which the heat production is shown in Fig. 6 as simulated with CEMHYD3D v.3∗. Compared to the experimentally determined heat production, the simulated one increased too fast.

From the very beginning pozzolanic hydration products (pozzolanic C—S—H and stratlingite (C_2AS_8)) were formed in the simulation, much more rapidly than in case of BFS. At 3 days, 9.50 g of FA has reacted per 100 g of cement (CEMHYD3D v.3∗), while less than 2 g would be expected for a composite cement with an f/b ratio of 0.50 [37]. This indicates that the reaction rate of the FA particles was too high. Therefore, adjusting the dissolution probabilities of the FA is preferred above changing the cycle-to-time calibration factor.

In CEMHYD3D v.3∗, the S is assumed to react with CH and water to form pozzolanic C—S—H. Although silica fume has stronger pozzolanic properties than FA, no distinction is made by CEMHYD3D v.3∗ between the reaction rate of S in FA and S in silica fume. Since the FA reaction is much slower, the initial probability for pozzolanic reactions (*ppozz*) was changed in CEMHYD3D v.3n from 0.05 to 0.005 corresponding with the one of BFS.

The ASG is assumed to react with CH and water to form C_2AS_8. The base dissolution probability of ASG amounts to 0.2 which is in the same order as those of the clinker phases (0.067–0.7). Again, since FA is not expected to react faster than BFS, the ASG dissolution probability was also decreased in CEMHYD3D v.3n to the value of BFS.

The presence of inert particles accelerates the C_3S reaction in CEMHYD3D v.3∗ based on the additional surface area which provides

Table 5
Diagnostics of the PLS models between measured velocity and simulated microstructure parameters: RMSEC (%), R^2_{loo} (–) and R^2_{split} (–).

Number of LV's		1	2	3	4	5	6	7	8	9	10
Degree of hydration (cement)	RMSEC	2.15	1.71	1.49	1.19	0.88	0.74	0.58	0.39	0.31	0.30
	R^2_{loo}	0.97	0.98	0.98	**0.98**	0.99	0.99	0.99	0.99	0.99	0.99
	R^2_{split}	0.71	0.88	0.96	**0.97**	0.93	0.93	0.93	0.94	0.94	0.94
Degree of hydration (total binder)	RMSEC	3.13	3.02	2.6	2.47	2.23	1.18	0.65	0.45	0.36	0.28
	R^2_{loo}	0.85	**0.87**	0.79	0.73	0.69	0.5	0.55	0.58	0.62	0.63
	R^2_{split}	0.25	**0.59**	−1.31	−2.41	−4.63	−2.35	−1.58	−0.97	−0.96	−0.89
Solid percolation	RMSEC	7.74	5.60	4.26	3.15	2.68	2.52	2.43	2.32	2.26	2.23
	R^2_{loo}	0.79	**0.89**	0.93	0.95	0.96	0.96	0.96	0.96	0.96	0.96
	R^2_{split}	0.78	**0.82**	0.77	0.73	0.61	0.60	0.61	0.65	0.67	0.68
Pore space percolation	RMSEC	0.62	0.58	0.56	0.45	0.41	0.32	0.15	0.08	0.05	0.04
	R^2_{loo}	−2.05	−1.01	−1.85	−1.34	−0.95	−2.06	−0.73	−0.38	−0.12	0.04
	R^2_{split}	−57.9	−123	−31.4	−46.0	−42.1	−66.8	−54.6	−36.6	−42.0	−32.9
Hydration products I formed (CH, AFm)	RMSEC	0.70	0.68	0.64	0.61	0.53	0.32	0.14	0.11	0.06	0.06
	R^2_{loo}	0.86	**0.75**	0.69	0.60	0.54	0.39	0.54	0.56	0.62	0.63
	R^2_{split}	0.50	**0.74**	−0.79	−2.33	−5.08	−2.07	−0.91	−0.45	−0.44	−0.37
Hydration products II formed (C—S—H,...)	RMSEC	1.79	1.73	1.53	1.44	1.31	0.71	0.38	0.31	0.24	0.22
	R^2_{loo}	0.89	**0.91**	0.85	0.82	0.77	0.65	0.7	0.72	0.75	0.76
	R^2_{split}	0.43	**0.80**	−0.75	−1.59	−3.46	−1.61	−1.14	−0.44	−0.43	−0.37

Table 6
Diagnostics of the PLS models between measured energy ratio and simulated microstructure parameters: RMSEC (%), R^2_{loo} (–) and R^2_{split} (–).

Number of LV's		1	2	3	4	5	6	7	8	9	10
Degree of hydration (cement)	RMSEC	2.60	1.71	1.25	1.17	1.11	1.02	0.89	0.84	0.78	0.72
	R^2_{loo}	0.96	**0.97**	0.98	0.98	0.98	0.98	0.97	0.98	0.97	0.97
	R^2_{split}	0.87	**0.88**	0.71	0.70	0.82	0.87	0.87	0.87	0.65	0.57
Degree of hydration (total binder)	RMSEC	3.11	2.79	2.51	2.27	1.73	1.68	1.45	1.16	1.07	0.79
	R^2_{loo}	0.82	**0.79**	0.79	0.46	0.51	0.50	0.82	0.68	0.60	0.59
	R^2_{split}	−0.38	**0.52**	−0.28	−0.16	−0.15	0.2	−0.18	−0.12	−0.19	0.28
Solid percolation	RMSEC	8.11	5.29	4.33	3.59	3.19	2.58	2.34	2.09	1.89	1.73
	R^2_{loo}	0.77	**0.90**	0.93	0.95	0.96	0.97	0.97	0.97	0.97	0.97
	R^2_{split}	0.62	**0.81**	0.69	0.48	0.34	0.32	0.25	0.37	0.15	−0.36
Pore space percolation	RMSEC	0.78	0.61	0.50	0.46	0.42	0.38	0.33	0.30	0.26	0.17
	R^2_{loo}	−1.77	−2.61	−1.12	−0.15	−0.10	−0.30	−1.52	−4.51	−10.2	−17.7
	R^2_{split}	−408	−56.9	−377	−312	−94.3	−98.8	−107	−93.1	−497	−702
Hydration products I formed (CH, AFm)	RMSEC	0.80	0.67	0.58	0.53	0.47	0.40	0.35	0.29	0.25	0.18
	R^2_{loo}	0.59	**0.58**	0.68	0.56	0.57	0.59	0.82	0.73	0.28	0.27
	R^2_{split}	−0.01	**0.54**	0.15	0.24	0.24	0.40	−0.22	−0.08	0.39	0.51
Hydration products II formed (C—S—H,...)	RMSEC	1.88	1.60	1.43	1.30	1.07	0.97	0.84	0.69	0.64	0.47
	R^2_{loo}	0.84	**0.83**	0.85	0.75	0.75	0.76	0.90	0.81	0.64	0.60
	R^2_{split}	−0.19	**0.71**	0.19	0.29	0.21	0.46	0.05	0.09	−0.10	0.55

nucleation sites for C—S—H and CH deposition. However, when cement is mixed with FA, the FA surface is proven by Fajun et al. [38] to act like a calcium sink. The Ca^{2+} ions in the pore solution are removed by the aluminium ions on the FA surface, preferentially forming ettringite. The Ca^{2+} concentration in the pore solution is hereby decreased during the first 6–10 h of the hydration, retarding the formation of a Ca-rich surface layer on the clinker minerals and the nucleation of C—S—H and CH [39]. Therefore, the

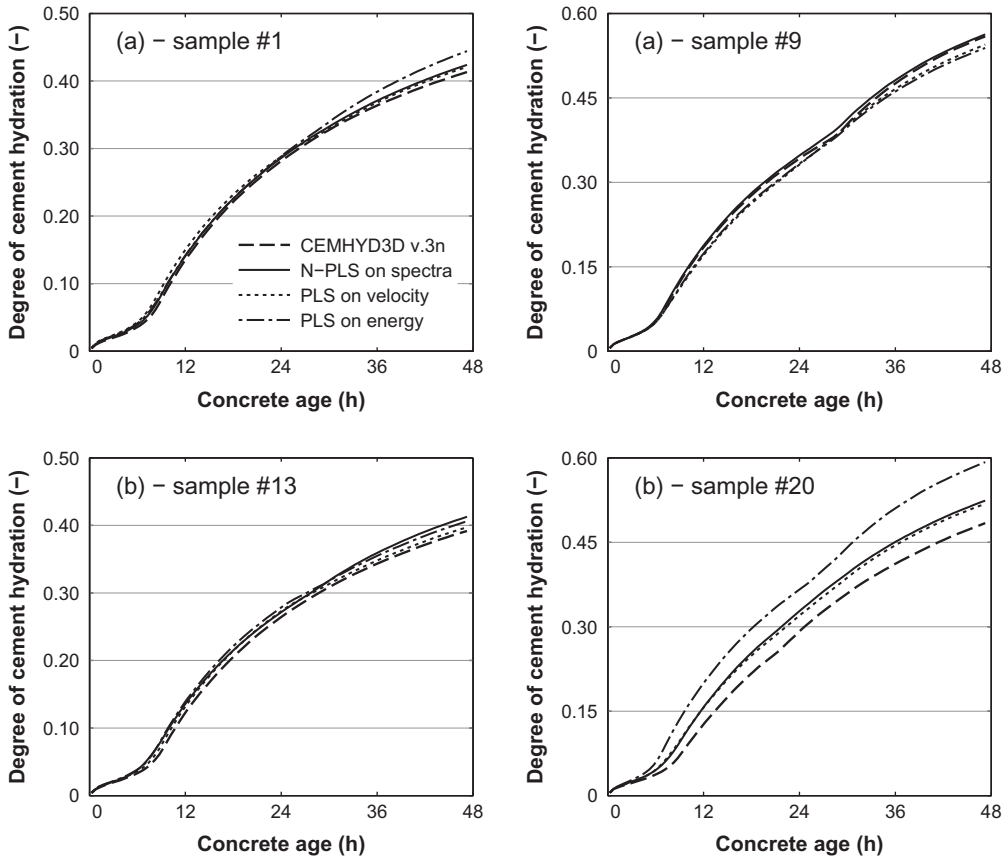

Fig. 8. Degree of hydration of the cement paste fraction vs. concrete age, simulated by CEMHYD3D v.3n and predicted with the (N-)PLS model on the p-wave velocity, energy ratio and frequency spectra measurements. The predictions were performed during cross-validation according to the (a) leave-one-out method and (b) split-half method.

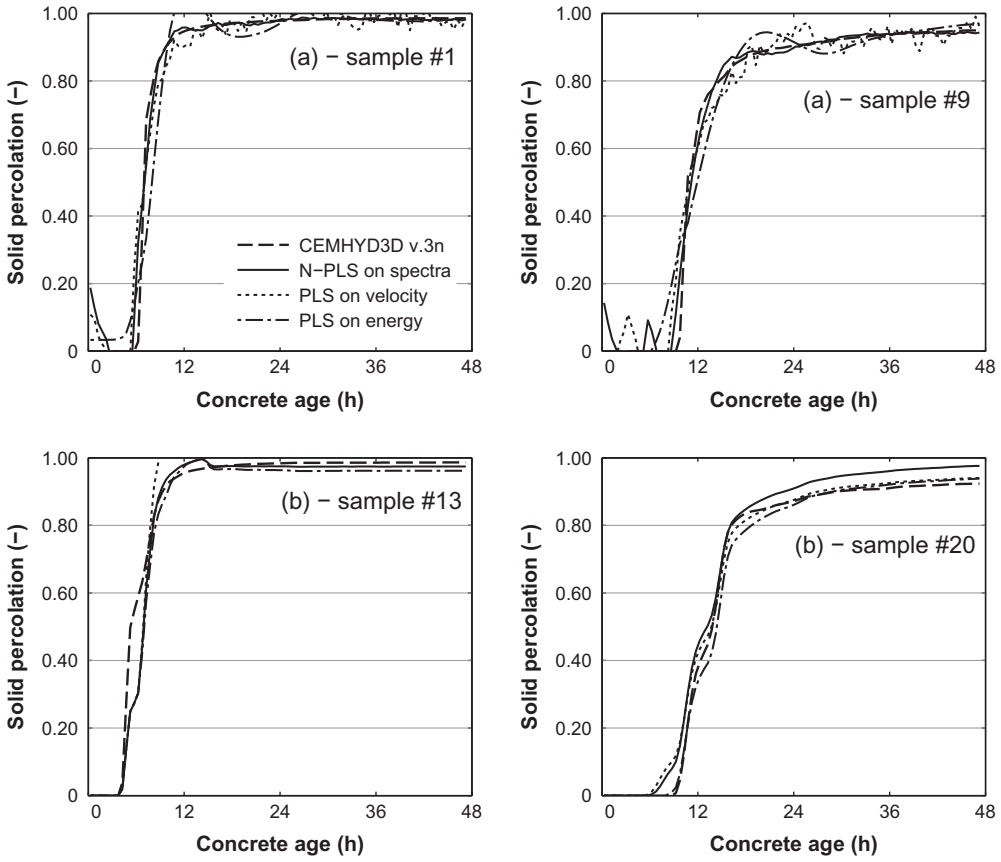

Fig. 9. Solid percolation of the cement paste fraction vs. concrete age, simulated by CEMHYD3D v.3n and predicted with the (N-)PLS model on the p-wave velocity, energy ratio and frequency spectra measurements. The predictions were performed during cross-validation according to the (a) leave-one-out method and (b) split-half method.

acceleration of the C_3S reaction due to heterogeneous nucleation on the inert FA particle surfaces was deleted from the source code in CEMHYD3D v.3n.

3.4. Validation of the reaction of FA in CEMHYD3D v.3n

The reduction of the pozzolanic activity, ASG dissolution probability and heterogeneous nucleation on inert particles lead to a better fit of the 50% FA mixture as shown in Fig. 6. With these adjustments to the model, 0.9 g of FA has reacted per 100 g cement at 3 days (CEMHYD3D v.3n), which agrees with the observations summarised by Taylor [37].

Fig. 7 shows the simulated heat production during hydration for all FA cement pastes. As with the BFS simulations, the second peak occurred approximately 2 h earlier compared to the experimental results. Contrary to the BFS simulations, the third peak is however not caused by the reaction of the mineral addition, but by the transformation of ettringite into monosulphate and an additional increase in C_3S hydration due to the stepwise increase in pH, discussed above. A discontinuity occurred after approximately 24 h for all the FA mixtures. The simulated cumulative heat production curves approximately coincide with the measured curves.

Table 3 compares the phase fractions at 2 days based on both the pixel counts of the CEMHYD3D v.3n simulations and the BSE images taken by Baert [15] which correspond well.

Fig. 5b shows the CH change in the FA mixtures as measured by Baert [15] with DTA-TGA and simulated with CEMHYD3D v.3n. Analogously to the BFS mixtures, CEMHYD3D v.3n estimated the CH content higher than DTA-TGA. As mentioned above, the latter method tends to underestimate the CH. Generally, the simulation and experimental results agree well for both FA and BFS during the first 2 days.

4. Predicting microstructure parameters with ultrasonic measurements

To study the microstructure development, six parameters related to this phenomenon were simulated with CEMHYD3D v.3n and related to the ultrasonic measurements by multi-way and multi-variate regression. The microstructure parameters are not scalars, but vectors giving the change of the quantity as the concrete setting proceeds. For every microstructure parameter, a separate N-PLS model had to be constructed between the measured frequency spectra ($\underline{\mathbf{X}}$) and this simulated parameter ($\mathbf{Y}$). To select the optimum number of LV's, the model diagnostics for an increasing number of components are shown in Table 4. Analogously, a PLS model was constructed between the measured ultrasonic velocity or energy ratio ($\mathbf{X}$) and every microstructure parameter ($\mathbf{Y}$). These model diagnostics are shown in Tables 5 and 6, respectively.

4.1. Degree of hydration

The degree of hydration of both cement (OPC) and total binder (OPC and addition) were used as $\mathbf{Y}$ matrix. All the ultrasonic parameters showed a good relation with the degree of cement hydration. The best prediction was achieved with the velocity measurements (Table 5, 4LV's, $R^2_{loo} = 0.98$, $R^2_{split} = 0.97$), but the models based on the frequency spectra (Table 4, 2LV's, $R^2_{loo} = 0.99$, $R^2_{split} = 0.91$) or the energy ratio (Table 6, 2LV's,

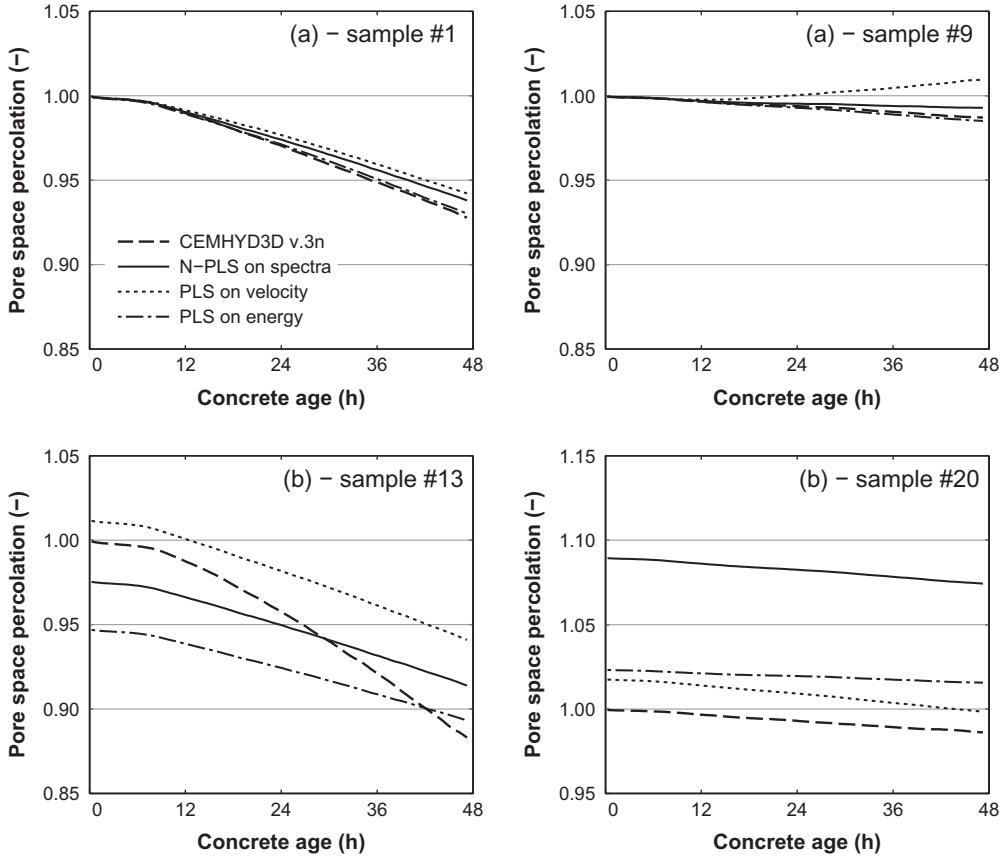

Fig. 10. Pore space percolation of the cement paste fraction vs. concrete age, simulated by CEMHYD3D v.3n and predicted with the (N-)PLS model on the p-wave velocity, energy ratio and frequency spectra measurements. The predictions were performed during cross-validation according to the (a) leave-one-out method and (b) split-half method.

$R^2_{loo} = 0.97,\ R^2_{split} = 0.88$) performed almost equally well. An example of two samples for both the leave-one-out and split-half cross-validation is given in Fig. 8. Except for sample #20 (split-half), the predictions and the simulations almost coincide.

The predictions of the degree of total binder hydration were less accurate for all ultrasonic measurements. The best results were obtained with the frequency spectra (Table 4, 2LV's, $R^2_{loo} = 0.93,\ R^2_{split} = 0.63$). However, the difference with the velocity and energy ratio was again restricted.

The better prediction of the degree of cement hydration compared to the degree of total binder hydration is attributed to the smaller contribution of the mineral addition to the hydration and setting at early-ages. The small changes in the hydration degree of the mineral addition are more difficult to predict accurately than the larger changes in cement hydration degree.

4.2. Solid percolation

Similar to the degree of hydration, the solid percolation related well to all ultrasonic parameters. The best predictions were achieved if the entire frequency spectra were considered (Table 4, 2LV's, $R^2_{loo} = 0.93, R^2_{split} = 0.86$), but also the velocity (Table 5, 2LV's, $R^2_{loo} = 0.89, R^2_{split} = 0.82$) and energy ratio (Table 6, 2LV's, $R^2_{loo} = 0.90, R^2_{split} = 0.81$) predictions were accurate. The predictions of new compositions seemed to benefit from the extra information in the frequency spectra compared to the energy ratio. The change of the solid percolation as simulated by CEMHYD3D v.3n and predicted with the (N-)PLS models are illustrated by two samples in Fig. 9 for both the leave-one-out method and split-half method.

The fraction of percolated solid particles was initially 0, which is difficult to predict since the ultrasonic parameters already increased from the start of the measurements. This initial increase is attributed to factors which have no or little influence on the actual stiffening process. In mixtures with thixotropic behaviour, thixotropy can affect the very early ultrasonic registrations. In traditional concrete mixtures, a combination of factors such as air bubble migration [7], internal settling [5], workability loss and ettringite formation [40] affects the measurements.

The ultrasonic quantities still increase after percolation due to the formation of additional hydration products, filling the pore space. Therefore, also the constant value of nearly 1 after percolation is difficult to predict and the regression curves fluctuate around it. Nevertheless, the sudden increase in percolated fraction is well predicted by the (N-)PLS models.

4.3. Pore space depercolation

Rapoport et al. [8] suggested that also the pore space depercolation might influence the ultrasonic measurements during the setting of cementitious materials. However, compared to the solid percolation, the fraction of percolated pores changed much less during the first 48 h (e.g. from 1 to 0.925 for sample #1, Fig. 10). Although a rigid framework of connected solid particles is formed during the first day after mixing, a continuous network of pores also remains present in this porous material. According to Ye [41] depercolation of the capillary porosity does not occur in cement pastes with a w/c ratio above 0.3, even at ages up to 1 year. Contrary to the suggestion of Rapoport et al. [8], the effect of pore space depercolation on early-age ultrasonic measurements might

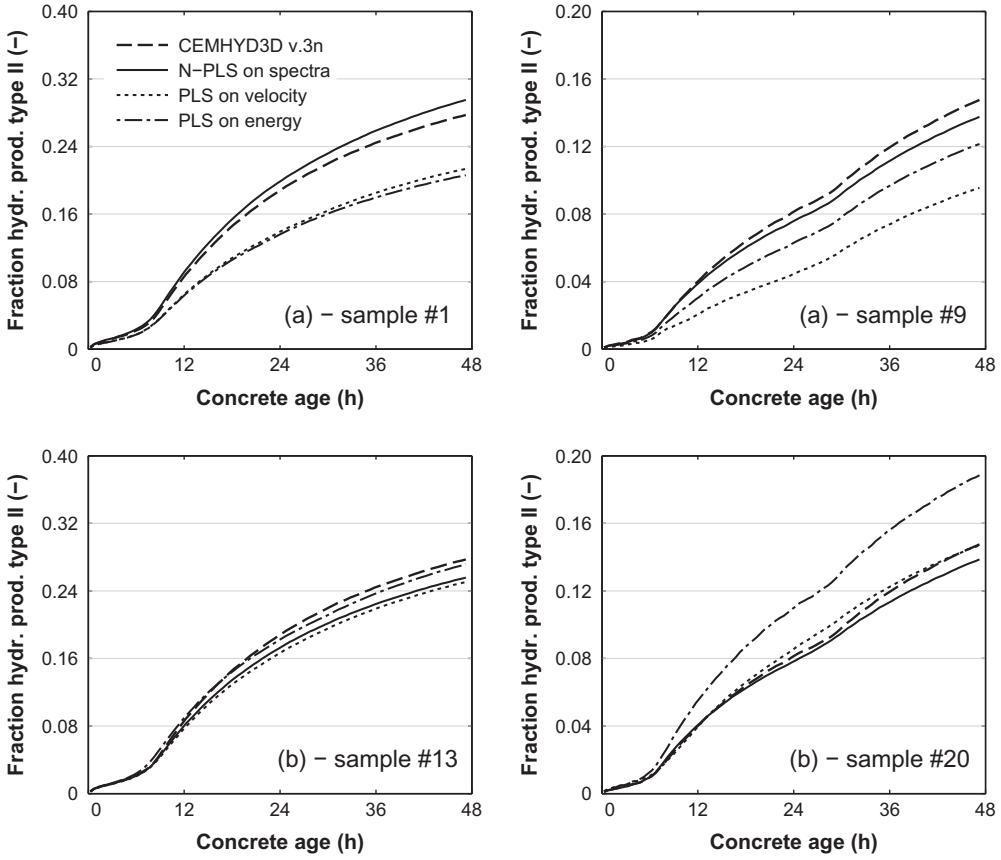

Fig. 11. Formation of type II hydration products (C—S—H, AFt, C_3AH_6) vs. concrete age, simulated by CEMHYD3D v.3n and predicted with the (N-)PLS model on the p-wave velocity, energy ratio and frequency spectra measurements. The predictions were performed during cross-validation according to the (a) leave-one-out method and (b) split-half method.

be minor. This is confirmed by the multi-way regression analysis. Both the leave-one-out and split-half cross-validation indicated a poor prediction of the pore space percolation with even negative R^2 values. This is also clearly illustrated by the differences in the curves of Fig. 10.

4.4. Formation of hydration products

The formation of hydration products is strongly related to the degree of hydration. Since good results were achieved for the latter, the formation of hydration products is also expected to be predicted well by the (N-)PLS modelling.

The change of the fraction type I hydration products (mainly CH) was best predicted by the model based on the frequency spectra (Table 4, 2LV's, $R^2_{loo} = 0.82, R^2_{split} = 0.88$) and worst by the energy ratio (Table 6, 2LV's, $R^2_{loo} = 0.58, R^2_{split} = 0.54$). Also the formation of type II hydration products (mainly C—S—H) was best predicted by the frequency spectra model (Table 4, 2LV's, $R^2_{loo} = 0.93, R^2_{split} = 0.82$), but the difference with the energy ratio (Table 6, 2LV's, $R^2_{loo} = 0.83, R^2_{split} = 0.71$) was much smaller.

The formation of type II products was thus mostly better predicted than of type I. For the mixtures with BFS or FA, the CH formed during the cement hydration is consumed by the reaction of the additions. During these reactions new C—S—H products are formed. The reduction of the fraction CH can therefore impossibly be detected by the ultrasonic method which mainly measures the change in stiffness of the specimen. The formation of C—S—H is more continuous and thus better related to the stiffness evolution.

Fig. 11 shows some examples from the leave-one-out and split-half cross-validation for the prediction of type II hydration product fractions. The good prediction by the frequency spectra is illustrated by these examples.

5. Conclusions

Ultrasonic measurements on concrete and mortar samples during their setting process can be related to the changes of fundamental microstructure parameters such as the degree of cement hydration, the solid percolation and the formation of hydration products. This relation was established by comparing the results of ultrasonic measurements to the microstructure development as simulated with an adjusted version of the pixel model CEMHYD3D.

First, a better simulation of the BFS reaction in CEMHYD3D was achieved by introducing an additional parameter (pH slag factor) to consider the different response of OPC and BFS to pH changes of the pore solution. In addition, the acceleration of the alite reaction in presence of inert FA particles was removed from the source code as tests with the isothermal calorimeter and SEM images could not confirm this heterogeneous nucleation. Although the new model sufficed for this study, the model can be further improved by making these adjustments dependent on the characteristics of the mineral additive, since merely one type of BFS and FA were tested in this research.

The simulated microstructure changes were then compared to the results of ultrasonic p-wave transmission tests on the corresponding concrete samples by multi-variate and multi-way regression analysis. Most microstructure parameters simulated by CEMHYD3D could best be related to the measured frequency spectra. However, the difference in prediction error compared to the

regression models based on the velocity and energy ratio is restricted. Thus, the measurement of the entire frequency spectra is not proven to add information about the microstructure development compared to the more simple velocity and energy measurements. The percolation of solid particles, the microstructure parameter most related to the setting, can be predicted by the ultrasonic measurements. However also other factors affect the ultrasonic signals since the formation of hydration products (especially C—S—H) and the hydration degree were even better predicted. Contrarily, no correlation could be found between the change in pore space percolation and the ultrasonic results.

Acknowledgements

As a Research Assistant of the Research Foundation – Flanders (FWO – Vlaanderen), the author wants to thank the foundation for the financial support. Regarding the data acquisition on the concrete mixtures and calorimetric, SEM and TGA-DTA measurements, Elke Gruyaert and Gert Baert are gratefully acknowledged. Finally, the author expresses his gratitude to Dale Bentz for the introduction to CEMHYD3D and the advice.

References

[1] Robeyst N, Grosse CU, De Belie N. Monitoring fresh concrete by ultrasonic transmission measurements: exploratory multi-way analysis of the spectral information. Chemometr Intell Lab Syst 2009;95(1):64–73.
[2] Robeyst N, Grosse CU, De Belie N. Measuring the change in ultrasonic p-wave energy transmitted in fresh mortar with additives to monitor the setting. Cement Concrete Res 2009;39(10):868–75.
[3] Robeyst N, Gruyaert E, Grosse CU, De Belie N. Monitoring the setting of concrete containing blast-furnace slag by measuring the ultrasonic p-wave velocity. Cement Concrete Res 2008;38(10):1169–76.
[4] Reinhardt HW, Grosse CU. Continuous monitoring of setting and hardening of mortar and concrete. Constr Build Mater 2004;18(3):145–54.
[5] Voigt T, Grosse C, Sun Z, Shah SP, Reinhardt HW. Comparison of ultrasonic wave transmission and reflection measurements with P- and S-waves on early age mortar and concrete. Mater Struct 2005;38(282):729–38.
[6] Lee HK, Lee KM, Kim YH, Yim H, Bae DB. Ultrasonic in-situ monitoring of setting process of high-performance concrete. Cement Concrete Res 2004;34(4):631–40.
[7] Ye G. Experimental study and numerical simulation of the development of the microstructure and permeability of cementitious materials. Delft: Technical University of Delft, PhD; 2003.
[8] Rapoport JR, Popovics JS, Kolluru SV, Shah SP. Using ultrasound to monitor stiffening process of concrete with admixtures. ACI Mater J 2000;97(6):675–83.
[9] van Breugel K. Simulation of hydration and formation of structure in hardening cement based materials. Delft: Technical University of Delft (TUDelft), PhD; 1991.
[10] Bentz D. Modelling cement microstructure: pixels, particles and property prediction. Mater Struct 1999;32:187–95.
[11] van Breugel K. Modelling of cement-based systems – the alchemy of cement chemistry. Cement Concrete Res 2004;34(9):1661–8.
[12] Bentz D. CEMHYD3D: a three-dimensional cement hydration and microstructure development modeling package, version 3.0. NISTIR 2005; 7232.
[13] Schwartzentruber A, Catherine C. La méthode du mortier de béton équivalent (MBE) – Un nouvel outil d'aide à la formulation des bétons adjuvantés. Matériaux et Constructions 2000;33:475–82.
[14] Jones R. Non-destructive testing of concrete. London: Cambridge University Press; 1962.
[15] Baert G. Physico-chemical interactions in Portland cement-(high volume) fly ash binders. Ghent: Ghent University, PhD; 2009.
[16] Gruyaert E, Van den Heede P, De Belie N. Acid resistance of concrete containing blast-furnace slag related to microstructural and physico-chemical parameters. Cement Concrete Res, submitted for publication.
[17] Gruyaert E, Robeyst N, De Belie N. Modelling the hydration heat of Portland cement blended with blast-furnace slag. In: Bílek V, Kersner Z, editors. 3rd International symposium on non-traditional cement and concrete. Brno; 2008. p. 76–85.
[18] Reinhardt HW, Grosse CU, Herb A, Bernd W, Schmidt G, Method for examining a solidified and/or hardening material using ultrasound, receptacle and ultrasound sensor for carrying out the method, United States Patent. Germany: Universität Stuttgart; 2003.
[19] Pane I, Hansen W. Investigation of blended cement hydration by isothermal calorimetry and thermal analysis. Cement Concrete Res 2005;35(6):1155–64.
[20] Stutzman P. Scanning electron microscopy imaging of hydraulic cement microstructure. Cement Concrete Compos 2004;26(8):957–66.
[21] Bentz D, Stutzman P, Haecker C, Remond S. SEM/X-ray imaging of cement-based materials. In: Pietersen HS, Larbi JA, Janssen HHA, editors. 7th Euroseminar: microscopy applied to building materials. Delft; 1999. p. 457–66.
[22] Bentz D. A three-dimensional cement hydration and microstructure program. I. Hydration rate, heat of hydration and chemical shrinkage. NISTIR 1995; 5756.
[23] Bentz D, Remond S. Incorporation of fly ash into a 3-D cement hydration microstructure model. NISTIR 1997; 6050.
[24] Bentz D. CEMHYD3D: a three-dimensional cement hydration and microstructure development modeling package, version 2.0. NISTIR 2000; 6485.
[25] Chen W, Brouwers HJH, Shui ZH. Three-dimensional computer modeling of slag cement hydration. J Mater Sci 2007;42(23):9595–610.
[26] Haecker CJ, Garboczi EJ, Bullard JW, Bohn RB, Sun Z, Shah SP, et al. Modeling the linear elastic properties of Portland cement paste. Cement Concrete Res 2005;35(10):1948–60.
[27] Bro R. Multi-way calibration: multi-linear PLS. J Chemometr 1996;10(1):47–62.
[28] Smilde A, Bro R, Geladi P. Multi-way analysis – applications in the chemical sciences. Chichester: John Wiley and Sons; 2004.
[29] Wise BM, Gallagher NB, Bro R, Shaver JM, Windig W, Koch RS. PLS_Toolbox Version 3.5 for use with MATLAB™ (Manual).Eigenvector Research Inc.; 2005.
[30] Durante C, Cocchi M, Grandi M, Marchetti A, Bro R. Application of N-PLS to gas chromatographic and sensory data of traditional balsamic vinegars of modena. Chemometr Intell Lab Syst 2006;83(1):54–65.
[31] Mysen BO. Structure and properties of silicate melts. Amsterdam: Elsevier; 1988.
[32] Chen W. Hydration of slag cement – theory, modeling and application. Enschede: University of Twente, PhD; 2006.
[33] Wolter A, Frischat GH, Olbrich E. Investigation of granulated blast furnace slag (gbfs) reactivity by SNMS. In: Grieve G, Owens G, editors. Proceedings of the 11th ICCC, vol. vol 4. Durban, South Africa: Cement and Concrete Institute; 2003. p. 1866–77.
[34] Odler I, Dörr H. Early hydration of tricalcium silicate I. Kinetics of the hydration process and the stoichiometry of the hydration products. Cement Concrete Res 1979;9(2):239–48.
[35] Bentur A, Berger RL. Chemical composition of C—S—H gel formed in the hydration of calcium silicate pastes. J Am Ceram Soc 1979;62(3):117–20.
[36] Shebl FA, Helmy FM, Ludwig U. A new approach on the hydration mechanism of tricalcium silicate. Cement Concrete Res 1985;15(5):747–57.
[37] Taylor H. Cement chemistry. London: Thomas Telford Publishing; 1990.
[38] Fajun W, Grutzeck MW, Roy DM. The retarding effects of fly ash upon the hydration of cement pastes: the first 24 hours. Cement Concrete Res 1985;15(1):174–84.
[39] Mishra SR, Kumar S, Park A, Rho J, Losby J, Hoffmeister BK. Ultrasonic characterization of the curing process of PCC fly ash–cement composites. Mater Charact 2003;50(4–5):317–23.
[40] Kamada T, Uchida S, Rokugo K. Nondestructive evaluation of setting and hardening of cement paste based on ultrasonic propagation characteristics. J Adv Concr Technol 2005;3(3):343–53.
[41] Ye G. Percolation of capillary pores in hardening cement pastes. Cement Concrete Res 2005;35(1):167–76.